Dalton Transactions

Cite this: *Dalton Trans.*, 2012, **41**, 2264

www.rsc.org/dalton

PAPER

Exploring the rotational isomerism in non-classical Wells–Dawson anions $\{W_{18}X\}$: a combined theoretical and mass spectrometry study†

Laia Vilà-Nadal,[a,b] Scott G. Mitchell,[a] De-Liang Long,[a] Antonio Rodríguez-Fortea,[b] Xavier López,[b] Josep M. Poblet*[b] and Leroy Cronin*[a]

Received 12th October 2011, Accepted 6th December 2011
DOI: 10.1039/c2dt11919f

We present a combined theoretical and mass spectrometry study of the rotational isomerism of the non-classical Wells–Dawson anions. The structure is larger than the Keggin anion and six geometric isomers are predicted (α, β, γ, α*, β*, γ*) on the basis of structural arguments. This work explores the geometrical differences between the isomers and evaluates the stability of these unusual clusters based upon the inclusion of the different heteroatoms. We connect the theoretical results with experimental studies by exploring the fragmentation of the parent clusters by electrospray-ionisation mass spectrometry (ESI-MS). Both approaches show a general stability trend that can be postulated as follows: γ* > β* > α* > α ≫ β > γ where the isomers γ*, β* and α are the only anions of this type known to have been synthesised.

Introduction

Polyoxometalates (POMs)[1] are an outstanding family of compounds, well known for their huge structural diversity,[2] interesting catalytic activities[3] and rich electrochemistry.[4] POMs are comprised of metal oxide building blocks with a general formula $\{MO_x\}_n$, where M = Mo, W, V, and sometimes Nb and x = 3–7.[5] The embedding of tetrahedral ($[SO_4]^{2-}$, $[PO_4]^{3-}$, $[SiO_4]^{4-}$), octahedral ($[IO_6]^{5-}$, $[TeO_6]^{6-}$) or pyramidal ($[SO_3]^{2-}$, $[BiO_3]^{3-}$) anions in the POM structure leads to the subfamily of heteropolyoxometalates (HPOMs). From a structural point of view, POMs are highly ordered clusters with additional architectures arising from the existence of various isomeric forms, notably in the common $[XM_{12}O_{40}]^{q-}$ Keggin[6] and $[X_2M_{18}O_{62}]^{2q-}$ Wells–Dawson (WD)[7] structures. Using the Clathrate model the WD anion can be viewed as two charged $[XO_4]^{q-}$ tetrahedral anions encapsulated by a neutral $[M_{18}O_{54}]$ cage, where X = P,[7] As,[8] S[9] or V[10] Conventionally, redox-inactive anions, such as $[SO_4]^{2-}$, $[PO_4]^{3-}$ and $[AsO_4]^{3-}$ are often used as templating anions in the formation of many WD clusters. However a recent strategy designed by us[11–13] to create new functional POMs involves the encapsulation of redox-active templates instead. By utilising $[SO_3]^{2-}$, $[SeO_3]^{2-}$, $[TeO_6]^{6-}$, and $[IO_6]^{5-}$ anions as templates, several new types of redox-active non-classical WD HPOMs have been isolated. In three examples where X = W^{VI}, Te^{VI} or I^{VII} both anionic templates are replaced by one central templating octahedral anion, $[XO_6]^{p-}$ to give the $[W_{18}O_{56}(XO_6)]^{(4+p)-}$ $\{W_{18}X\}$ type POM. The first member of this family to be discovered was actually an isopolyanion $\{W_{19}\} = \{W_{18}W\}$ with a Wells–Dawson-type cage; the nineteenth tungsten is located at the centre of the cluster instead of the two tetrahedral heteroatoms that are usually found inside conventional Dawson clusters.[11] Structural analysis of the cluster shows that the nineteenth tungsten could be replaced by other elements, such as Sb^{V}, Te^{VI}, or I^{VII}. The anions β*-$[H_3W_{18}O_{56}(IO_6)]^{6-}$ embedded with high-valent iodine[12] and γ*-$[H_3W_{18}O_{56}(TeO_6)]^{7-}$ that captures the tellurate anion TeO_6^{6-} were discovered thereafter (Fig. 1).[13]

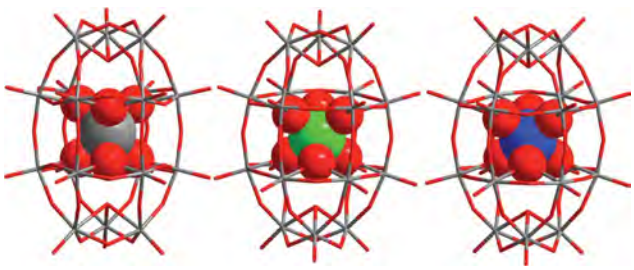

Fig. 1 Structures of the non-classical Wells–Dawson $\{W_{18}X\}$ type POM. The $\{W_{18}\}$ cages are shown as a wireframe and the central octahedral $\{XO_6\}$ group is represented as a space-filling model. Left: α-$[W_{18}O_{56}(WO_6)]^{10-}$. Middle: γ*-$[W_{18}O_{56}(XO_6)]^{10-}$ X = W^{VI} and Te^{VI}. Right: β*-$[W_{18}O_{56}(IO_6)]^{9-}$. Colour code for spheres and wires is the following, W = grey, O = red, Te = green, I = blue.

Although isomerism in POMs has been studied in isolated reports with their properties explored both experimentally and

[a]*WestCHEM, School of Chemistry, The University of Glasgow, Glasgow, UK, G12 8QQ. E-mail: L.Cronin@chem.gla.ac.uk; Fax: (+44) 141-330-4888; Tel: (+44) 141-330-6650; Web: http://www.croninlab.com*
[b]*Departament de Química Física i Inorgànica, Universitat Rovira i Virgili, c/Marcel·lí Domingo s/n, 43007, Tarragona, Spain. E-mail: josepmaria.poblet@urv.cat; Fax: (+34) 977-559-563; Tel: (+34) 977-559-569; Web: http://www.quimica.urv.es/w3qf/*

† Electronic supplementary information (ESI) available: information regarding CID-MS fragmentation experiments and DFT calculations. See DOI: 10.1039/c2dt11919f

computationally, some basic points are still unclear. However, tuning physical properties using the geometrical changes found for an isomer, such as the different location of a given atom (positional isomerism), or a rotation of a fragment of the molecule (rotational isomerism) would be interesting. Six isomers for the $[X_2M_{18}O_{62}]^{6-}$ anion (X = As^V, P^V; M = Mo^{VI}, W^{VI}) were postulated in 1970 by Baker and Figgis and named α, β, γ and α*, β*, γ*.[14] The same notation has been used for the $\{W_{18}X\}$ isomers, depicted in Fig. 2. Since heteroatoms As or P and I or Te are located either at the centre of the cluster (non-classical WDs) or symmetrically located on C_3 axis (classical WDs) their existence does not affect the symmetries of the clusters, therefore both the classic $[X_2M_{18}O_{62}]^{2q-}$ and non-classic $[W_{18}O_{56}(XO_6)]^{(4+p)-}$ WDs can share the same symmetrical system notations.

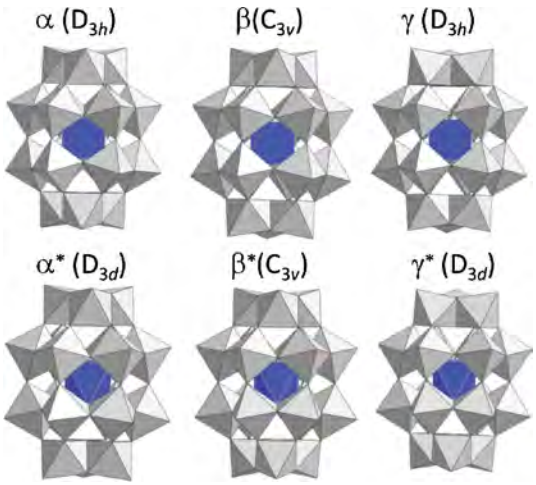

Fig. 2 The six rotational isomers of the non-classical Wells–Dawson $\{W_{18}X\}$ structure. Top: α, β, γ. Bottom: α*, β*, γ*.

As depicted in Fig. 2 and 3, all the α, β, γ isomers have a D_{3h} symmetric trigonal prism $[XO_6]^{p-}$ moiety inside the clusters, while all the α*, β*, γ* isomers have a D_{3d} symmetric trigonal antiprism $[XO_6]^{p-}$ moiety. The α-$[W_{18}O_{56}(XO_6)]^{(4+p)-}$ (X = W^{VI}, Te^{VI} and I^{VII}) isomer has a D_{3h} symmetric $\{W_{18}O_{54}\}$ cage shell and the whole cluster belongs to D_{3h} point group[15] in which all the oxo ligands of the $[XO_6]^{p-}$ moiety bridge pair of W atoms within square windows of the $\{W_9O_{34}\}$ half. The β anion, see Fig. 3 for more details, is derived from the α isomer by a formal rotation by π/3 of a polar (cap) W_3O_{13} group: the cluster symmetry is lowered to C_{3v}. A formal rotation by π/3 of the second polar M_3O_{13} group restores the symmetry plane and the point group D_{3h} for the γ isomer. If the two belt $\{\alpha\text{-}W_9O_{34}\}$ subunits are related through an inversion centre, as postulated by Wells[16] in 1945 for $[P_2W_{18}O_{62}]^{6-}$, the resulting anion named α* has a D_{3d} symmetric $\{W_{18}O_{54}\}$ cage shell and its cluster symmetry belongs to the D_{3d} point group. Rotation of one or both polar (cap) M_3O_{13} groups of this α* anion would generate the two remaining isomers, β* (C_{3v}) and γ* (D_{3d}) respectively.[17] As depicted in Table 1, five of the six isomers have been detected and solved by single crystal X-ray diffraction and only the α* isomer remains synthetically elusive. It is also worthy of note that there are two tetrahedral "voids" in the non-classical WDs at the positions that are typically occupied by the heteroatoms in conventional WD cluster anions, see Fig. 1. These positions are protonated and form H-bonds, similar to what

Table 1 Observed isomers for the classic $\{W_{18}X_2\}$ and non-classical $\{W_{18}X\}$ Wells–Dawson structures when M = W or Mo[a]

	Isomers					
Metal	α	β	γ	α*	β*	γ*
		Classic WD $\{(XO_4)_2M_{18}O_{54}\}$				
M = W	PO_4^{3-}[b]	PO_4^{3-}[c]	PO_4^{3-}[d]			PO_4^{3-}[e]
	AsO_4^{3-}[f]	AsO_4^{3-}[e]	AsO_4^{3-}[e]			SO_4^{2-}[g]
	SO_4^{2-}[h]					
M = Mo	PO_4^{3-}[i]					
	AsO_4^{3-}[j]					
	SO_4^{2-}[k]					
		Non-classical WD $\{(XO_3)_2M_{18}O_{54}\}$				
M = W	SO_3^{2-}[h]					
	BiO_3^{3-}[l]					
	AsO_3^{3-}[m]					
M = Mo	SO_3^{2-}[n]					
	$P_2O_7^{4-}$[o]					
		Non-classical WD $\{(XO_6)M_{18}O_{56}\}$[p]				
M = W	WO_6^{6-}[q]				IO_6^{5-}[r]	WO_6^{6-}[q]
						TeO_6^{6-}[s]

[a] Blank spaces correspond to non observed isomers. [b] Ref. 7 [c] Ref. 23. [d] Ref. 24. [e] Ref.8c [f] Ref.8a [g] Ref. 25. [h] Ref. 9. [i] Ref. 26. [j] Ref.8b [k] Ref. 27. [l] Ref. 28. [m] Ref. 29. [n] Ref. 30. [o] Ref. 31. [p] Anions with formula $\{(XO_6)M_{18}O_{56}\}$have not been observed for M = Mo. [q] Ref. 11. [r] Ref. 12. [s] Ref. 13.

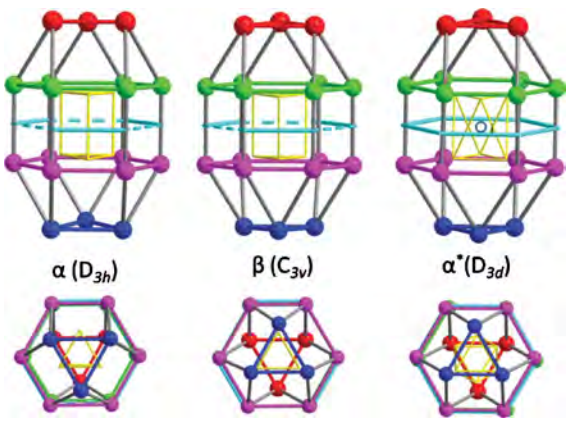

Fig. 3 Top: rationalisation of the 18 metal-centred α, β and α* Wells—Dawson non-classical structures. Bottom: vision along the C_3 axis. In the α isomer both CAP (red and blue) triads appear eclipsed along the C_3. On the contrary, the CAP triads appear staggered in the β and α* isomers. This is due to a π/3 rotation of the blue CAP in the α isomer that leads to the β anion. Another rotation of the red CAP in the β isomer will derive the γ isomer, not depicted here. The short-long alternation in the distances between the oxygen atoms that interconnect both BELT units, depicted in turquoise, is maintained in the α, β and γ isomers. If both CAP–BELT, $\{\alpha\text{-}W_9O_{34}\}$ subunits are related through an inversion centre "i", depicted in the figure, we obtain the α* isomer with a D_{3d} symmetry. In this case the distance alternation between central oxygens (turquoise) disappears. The same happens with β* and γ*, since the oxygens are related through the improper axis S_6. Like β and γ isomers, a π/3 rotation of the blue CAP in the α* isomer will lead to the β* and the rotation of both CAP (blue and red) to γ*. Note from the bottom figures, vision along the C_3 axis, that $[XO_6]^{p-}$ yellow octahedral appear eclipsed in α, β, consequently in γ isomers, whereas are staggered in α* and subsequently in β*, γ*.

is observed in the Keggin cluster $[H_2W_{12}O_{40}]^{6-}$ and the semi-vacant Dawson polyoxo-tungstate $[Ce\{P(H_4)W_{17}O_{61}\}_2]^{19-}$.[11]

A. F. Wells stated, in the early sixties, that *"there is still much to be learnt about the structures of these salts"* referring

Table 2 Relative energies (E_{rel}) with respect to the most stable isomer, HOMO–LUMO gaps and the X–O_{inner} distance for the six isomers of $[W_{18}O_{56}(XO_6)]^{(4+p)-}$ where X = W, Te and I, compared to the $[W_{18}O_{56}]^{4-}$ cage

		$[W_{18}O_{56}]^{4-a}$	$[W_{18}O_{56}(WO_6)]^{10-b}$			$[W_{18}O_{56}(TeO_6)]^{10-b}$			$[W_{18}O_{56}(IO_6)]^{9-b}$		
Isomer	Symmetry	ΔE_{rel} [c]	ΔE_{rel} [c]	H–L gap[d]	$d_{X-O_{inner}}$ [e]	ΔE_{rel} [c]	H–L gap[d]	$d_{X-O_{inner}}$ [e]	ΔE_{rel} [c]	H–L gap[d]	$d_{X-O_{inner}}$ [e]
α	D_{3h}	0.0	9.1	1.3	2.00	13.3	0.8	2.14	19.7	0.2	2.14
β	C_{3v}	1.9	13.0	1.2	2.01–1.99	18.0	0.8	2.14–2.13	24.7	0.1	2.12–2.13
γ	D_{3h}	0.0	16.1	1.2	2.00	21.3	0.8	2.14	26.2[f]	0.1	2.19
α*	D_{3d}	1.9	7.0	1.7	1.99	4.6	1.7	2.10	5.0	1.1	2.08
β*	C_{3v}	0.0	0.0	1.9	1.85–2.17	1.5	1.7	2.09–2.11	1.5	1.0	2.08–2.07
γ*	D_{3d}	1.8	0.1	1.6	1.99	0.0	1.6	2.10	0.0	1.0	2.08

[a] Geometry optimized BP86, gas phase. [b] Geometry optimized BP86/SES. [c] kcal mol^{-1}. [d] eV. [e] Å. [f] triplet.

to the iso- and heteropolyacid salts of polyoxometalates known at the time.[18] Since Dawson solved the crystal structure of α-$K_6[P_2W_{18}O_{62}]\cdot 14H_2O$[7a] there has been renewed and considerable effort during the last decades (see Table 1) to understand and control isomerism in POMs. At first glance, the α isomer in Table 1 appears as the most common structure, regardless of the heteroatom. Therefore the α configuration of the W_{18} 'box' is the most flexible among all isomers, being able to stabilise the classic $[XO_4]^{q-}$ and non-classic $[XO_3]^{q-}$, $[XO_6]^{p-}$ heteroanions. By observing the amount of blank spaces left in Table 1 and the fact that β* isomer is only obtained when the heteroanion is $[IO_6]^{5-}$, one can easily attempt to predict a stability order for the isomers (α > γ* > γ ≈ β > β* > α*), where α and γ* are most stable, and thus the most observed isomers. Significant contributions to this field have been made by Contant and Thouvenot, who have already discussed geometrical differences between isomers and the stability of γ*, stating that it is the most stable among the staggered structures.[8c] In a previous DFT study, Poblet and co-workers analysed the relative stability of the α and β isomers of the Wells–Dawson (WD) heteropolyanions.[19a] In a more recent DFT study by Su and co-workers the following stability trend has been found for isomers of $[P_2W_{18}O_{62}]^{6-}$ (α > β > γ > γ*> α*> β*).[20] Our aim here is to study, by means of DFT, the non-classical WD $\{W_{18}X\}$ and understand their preferences for certain conformations. We have complemented the theoretical study using electrospray-ionisation mass spectrometry (ESI-MS) experiments. Cronin and co-workers have recently demonstrated that a combination of cation-exchange and electrospray-ionisation mass spectrometry (ESI-MS) can be used as a versatile tool to elucidate the complete cluster composition, including the degree of protonation, as well as determining the relative proportions of the cluster species present in solution.[21] POM clusters represent ideal candidates for examination using high-resolution mass spectrometry since they are intrinsically charged and have characteristic isotopic envelopes, which can be precisely fitted to determine the exact formula.[22] In the present paper we will discuss the isomerism of the non-classical WD structure from a theoretical point of view.

Results and discussion

Isomerism for non-classical Dawson anions $\{M_{18}X\}$ α, β, γ, α*, β*, γ* when M = W

As a preliminary study we have analysed the relative stability of the six isomers of the classic Wells–Dawson (WD) $[X_2M_{18}O_{62}]^{2q-}$ heteropolyanions when X = P, As or S. Geometry optimisations with symmetry constraints performed on the six isomers of WD anion, when X = P, As and S, led to structures listed in Table S1 and Fig. S1.† For instance, the α isomer of As_2W_{18} was computed under the constraints of D_{3h} symmetry, whereas for the corresponding β isomer we have assumed the symmetry of the molecule is C_{3v}, *etc.* For the six isomers of $[P_2W_{18}O_{62}]^{6-}$, $[As_2W_{18}O_{62}]^{6-}$ and $[S_2W_{18}O_{62}]^{4-}$ we have obtained the same stability trend as Su and co-workers.[20] Here, we have extended that previous work towards the non-classical WD $\{W_{18}X\}$ anions to explore the effect of including the single central heteroanion.

Due to the presence of protons in $\{W_{18}X\}$ species, the full analysis of the isomerism in non-classical WD anions is more complex compared to their $\{W_{18}X_2\}$ analogues. At this initial stage, and for reasons of simplicity, we have not included protons in the $\{W_{18}\}$ cage, and consequently the charge of the anion has increased, *i.e.* instead of $[H_3W_{18}O_{56}(IO_6)]^{6-}$ we have studied the $[W_{18}O_{56}(IO_6)]^{9-}$species. Table 2 shows the relative energies with respect to the most stable isomer for the $[W_{18}O_{56}(XO_6)]^{(4+p)-}$ WD type isomer. We have first evaluated the relative stability of the six isomers considering only the $[W_{18}O_{56}]^{4-}$ cage without the internal anions $[XO_6]^{p-}$, observing the same trend as the $[W_{18}O_{54}]$ cage of classic WD isomers (see Table S1†). The six isomers for both cases, *i.e.* $[W_{18}O_{56}]^{4-}$ and $[W_{18}O_{54}]$, are quasi degenerate structures. So, the stability of one isomer is not determined by the stability of the cage, it strongly depends on the interactions of the encapsulated anion embedded within it.

From the results for $[W_{18}O_{56}(XO_6)]^{(4+p)-}$ when X = W, Te and I, it is interesting to point out that the α*, β* and γ* group of isomers is by far the more stable (more than 10 kcal mol^{-1}) than the group formed by the α, β and γ isomers. See in Table S1† that, for the classic WD structures, the most stable isomers are the α, β, γ and γ*. The main geometrical differences between the six non-classical isomers have been shown in Fig. 2. Here we would like to highlight that the internal oxygens for $[W_{18}O_{56}(XO_6)]^{(4+p)-}$ are *eclipsed* in isomers α, β, γ and *staggered* in α*, β*, γ* (see Fig. 4 bottom). This geometrical difference determines the relative stability of these isomers, the latter being, in general, more than 10 kcal mol^{-1} lower in energy than the former. In a previous paper, we analysed the stability trend of $\{W_{19}\}$ isomers from a theoretical point of view.[11] In contrast to these previous results we found that the D_{3h}-symmetric α isomer is more stable than the D_{3d}-symmetric γ* isomer. Despite the use of different codes in the analyses (Turbomole and ADF) the levels of theory used in both cases are comparable. However the omission of solvent

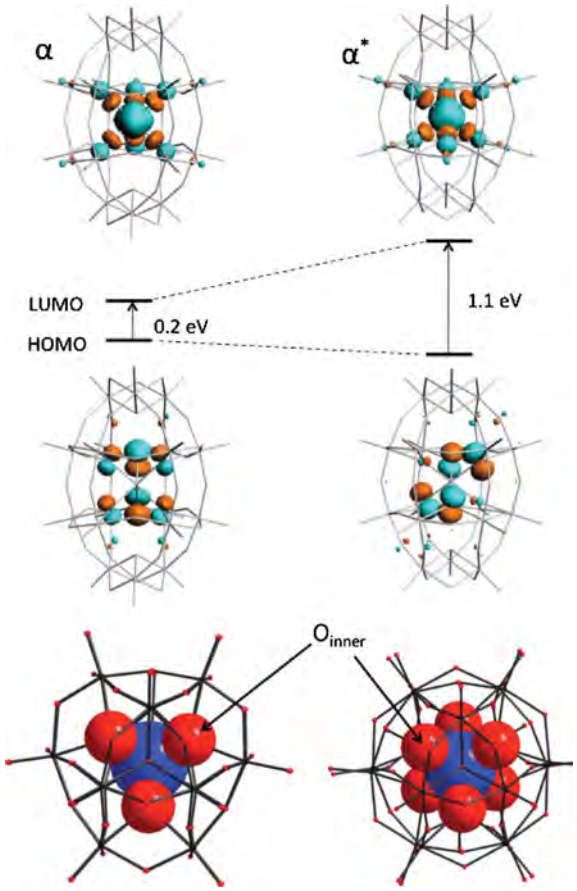

Fig. 4 Above: graphical representation of the HOMO–LUMO gap, in eV, for α (D_{3h}) and α* (D_{3d}) isomers of $[W_{18}O_{56}(IO_6)]^{9-}$. 3D representations for the HOMO (orbital delocalized over the inner oxygen atoms) and the LUMO (orbital delocalised over the I atom and the inner oxygen atoms). Below: Wells–Dawson-like structures $\{W_{18}X\}$ POM type, the $\{W_{18}\}$ cages are shown as sticks and the central $\{XO_6\}$ group is represented as space filling model, X: blue sphere; O: red sphere. Left: for the α isomer the inner oxygen atoms appear eclipsed; the same happens for the β and γ isomers. Right: for the α* isomer the inner oxygen atoms appear staggered as they are for β* and γ* isomers.

in previous calculations appears to be a key factor in establishing the correct relative stabilities of the POMs, and this is a plausible explanation for the differences encountered when comparing both stability trends.

The higher stability of isomers α*, β* and γ* in the non-classical structures can be easily rationalised from the analysis of the frontier orbitals. On one hand, the HOMO–LUMO (H–L) gaps are considerably larger for these isomers compared to α, β and γ isomers: ~0.9 eV in the case of X = Te, I and slightly smaller (~0.6 eV) in the case of X = W. On the other hand, we have also found geometrical differences in the $X–O_{inner}$ distances: they are larger (~0.05 Å, X = I) in the α, β, γ isomers than in α*, β*, γ*. Fig. 4 aims to summarise these observations for isomers α and α* in the case of $[W_{18}O_{56}(IO_6)]^{9-}$.

As shown in Table 2, the α isomer of the $[W_{18}O_{56}(IO_6)]^{9-}$ anion is about 21 kcal mol^{-1} higher in energy than the α* isomer. This high energy arises from the eclipsed conformation of the internal oxygen atoms. In fact, the HOMO lies quite high in energy and the H–L gap is rather small. Both factors are a sign of instability. As for α* isomer the 60° degrees rotation of one O_3 unit in the heterogroup $\{IO_6\}$ leads to a relaxation of the system and is associated with a stabilisation of the HOMO and a destabilisation of the LUMO, thus an increase of the H–L gap. This is due to the eclipsed disposition of inner O atoms in the α isomer.

The antibonding interactions among oxygen atoms in the HOMO of the α isomer are more important than in the HOMO of α*, where these interactions are minimised thanks to the staggered disposition of inner O atoms. The key parameter in the destabilisation for α* LUMO orbital is the distance between central atom and inner oxygen atoms. As we have said previously this distance is slightly smaller for α* isomer. Therefore, the antibonding X–O interactions in the LUMO are much more effective than those in the LUMO of the α isomers, thus becoming more destabilised than the α LUMO.

An average difference in stability around 7 kcal mol^{-1} was computed for several classical WD isomers that have been experimentally characterised in close agreement with recent results of Su and co-workers.[20] The values in Table 2 show that the α isomer of $[W_{18}O_{56}(WO_6)]^{10-}$ is 9 kcal mol^{-1} less stable than γ*. Both isomers have been observed experimentally, and building on our previous results for the classic WD system, we decided to explore role of protons in the relative stability of these molecules. We therefore modelled the protonation of the two μ_3-O atoms, which are the most basic, as observed in the electrostatic potential distribution map in Fig. 5.

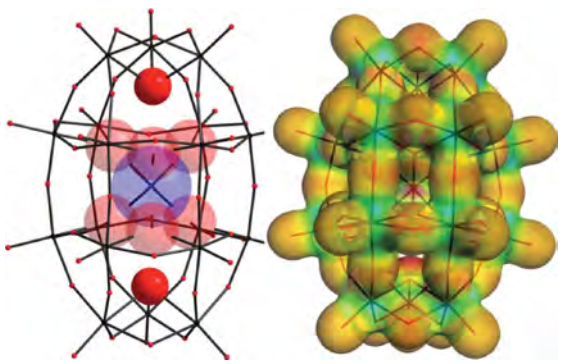

Fig. 5 Left: highlighted in bright red the two protonated μ_3-O. Right: image of the electrostatic potential for $[W_{18}O_{56}(WO_6)]^{10-}$ highlighting the μ_3-O electronegative sites. Coloured regions correspond to the following scale being (most negative) red < yellow < green < light blue < dark blue (most positive).

Protonation of the two internal μ_3-O atoms in $[W_{18}O_{56}(WO_6)]^{10-}$ has two noticeable consequences: a) it reduces the energy difference among all six isomers, five of them being in energy range lower than 5 kcal mol^{-1} and b) the computed geometries are closer to the experimental ones. We have also compared the distances between the two μ_3-O atoms from the X-ray structure and the computed protonated and non-protonated species, the results are shown in Table 3. For the non-protonated systems the distance between the two apical oxygen atoms was computed to be 7.9 Å. Upon diprotonation this distance is reduced by *ca.* 0.4 Å.

Stability insights arising from CID-MS fragmentation experiments

One of the great tasks for the synthetic chemist is the complete characterisation of new materials. The accurate determination

Table 3 Relative energies (E_{rel}) and distances between apical oxygen atoms for the diprotonated species of $[W_{18}O_{56}(XO_6)]^{q-}$ where X = W, Te and I

	$[H_2W_{18}O_{56}(WO_6)]^{8-}$			$[H_2W_{18}O_{56}(TeO_6)]^{8-}$			$[H_2W_{18}O_{56}(IO_6)]^{7-}$		
		$d_{O\cdots O}$[b]			$d_{O\cdots O}$[b]			$d_{O\cdots O}$[b]	
Isomer	E_{rel}[a]	X-ray	DFT	E_{rel}[a]	X-ray	DFT	E_{rel}[a]	X-ray	DFT
α	3.9	7.39	7.57 (7.92)	9.4			14.3		
β	4.8			14.5			18.6		
γ	12.4			16.6			[c]		
α*	4.0			7.1			7.0		
β*	0.0			3.7			3.1	7.47	7.53 (7.85)
γ*	1.1	7.35	7.57 (7.96)	0.0	7.39	7.64 (7.94)	0.0		

[a] Relative energies with respect to the most stable isomer in kcal mol^{-1}. [b] Distance between the two apical oxygen atoms in Å. In parenthesis the computed distances for the non protonated species. [c] We have not optimised the protonated geometry.

of formula and structure of most polyoxometalates can now be attained with relative ease. However, understanding the assembly process still represents a significant challenge: one that is crucial for further synthetic development and exploitation. The use of electrospray mass spectrometry (ESI-MS) to investigate POM systems, as a complementary technique to X-ray crystallography and NMR studies, has increased steadily over the last decade.[32–33] In this respect we recently have gone to great effort to demonstrate that electrospray (ESI-) and cryospray mass spectrometry (CSI-MS) are powerful analytical tools for studying complex metal oxides in the gas phase.[34] Very often, comprehensive studies not only allow the elucidation of chemical formula but also provide important insight into the key structural building blocks present in solution.[35] In this instance the observed data from fragmentation studies can be correlated to possible mechanisms of assembly of the clusters.[36] Although it may be said that fragmentation studies are generally limited with regards to the useful mechanistic information they provide on self-assembly, any such data that can be obtained may be used in postulating possible self-assembly mechanisms. In our previous work, ESI- and CSI-MS studies showed that many POM clusters retain their structural integrity in solution and, importantly, have helped us to unambiguously determine the extent of protonation of many discrete cluster types. Here we show how Collision-Induced Dissociation (CID) studies can be used to provide qualitative determination of cluster stability in combination with DFT studies and also provide possible assembly mechanisms.

As mentioned above, in the non-classical $\{W_{18}X\}$ clusters, the two tetrahedral cavities that are usually occupied by heteroatoms in conventional Wells–Dawson clusters are vacant, and the apical interior μ_3-O positions are protonated. Consequently, the structures for all four of the clusters are very similar, but only $((n\text{-}C_3H_7)_4N)_6[\gamma^*\text{-}H_4W_{18}O_{56}(W^{VI}O_6)]$ and $((n\text{-}C_3H_7)_4N)_7[\gamma^*\text{-}H_3W_{18}O_{56}(Te^{VI}O_6)]\cdot 4CH_3CN$ have identical cluster symmetry and differ only in the identity of the central atoms and protonation state. In order to evaluate the composition of the clusters in the gas phase and to simplify the MS experiments, all four clusters were prepared as *tetra*-propylamine salts ($((n\text{-}C_3H_7)_4N)^+$ = TPA^+). The principle peaks observed during the course of the CID experiments for all compounds were the plenary polyanions: namely for both $((n\text{-}C_3H_7)_4N)_6[\alpha\text{-}H_4W_{18}O_{56}(W^{VI}O_6)]$ and $((n\text{-}C_3H_7)_4N)_6[\gamma^*\text{-}H_4W_{18}O_{56}(W^{VI}O_6)]\cdot 3CH_3CN$ these were $((n\text{-}C_3H_7)_4N)_4[H_4W_{19}O_{62}]^{2-}$ (m/z 2617.3), $((n\text{-}C_3H_7)_4N)_3[H_4W_{19}O_{62}]^{3-}$ (m/z 1682.5) and $((n\text{-}C_3H_7)_4N)_2[H_4W_{19}O_{62}]^{4-}$ (m/z 1215.6) and $((n\text{-}C_3H_7)_4N)[H_4W_{19}O_{62}]^{5-}$ (m/z 935.2) (see Table S6† and Fig. 6). The associated plenary clusters for compounds $((n\text{-}C_3H_7)_4N)_6[\beta^*\text{-}H_3W_{18}O_{56}(I^{VII}O_6)]$ and $((n\text{-}C_3H_7)_4N)_7[\gamma^*\text{-}H_3W_{18}O_{56}(Te^{VI}O_6)]\cdot 4CH_3CN$ can also be identified (see Table S7 and Fig. S3†). The synthesis of $((n\text{-}C_3H_7)_4N)_6[\beta^*\text{-}H_3W_{18}O_{56}(I^{VII}O_6)]$ represented the first time that the $[I^{VII}O_6]^{5-}$ ion had been captured within a polyoxometalate and the first time that iodine, in its highest valence +7, had been included in a tungsten oxide cluster and fully characterised crystallographically. ESI-MS experiments in the original publication and references contained therein demonstrate that $[\beta^*\text{-}H_3W_{18}O_{56}(I^{VII}O_6)]^{6-}$ can be isolated as a pure polyoxometalate, with no co-crystallised $\{W_{19}\}$ species and can contain several protonation states (see Fig. S4 and Table S5†). In order to provide qualitative information on the stability of the $\{W_{18}X\}$ family, a series of CID ESI-MS experiments were investigated. The triple negatively-charged plenary cluster species in the mass spectra of all four compounds were targeted and fragmented successively by increasing the collision energy of the MS collision cell. Consequently, it was possible to monitor the exact collision energy required to completely fragment the triply

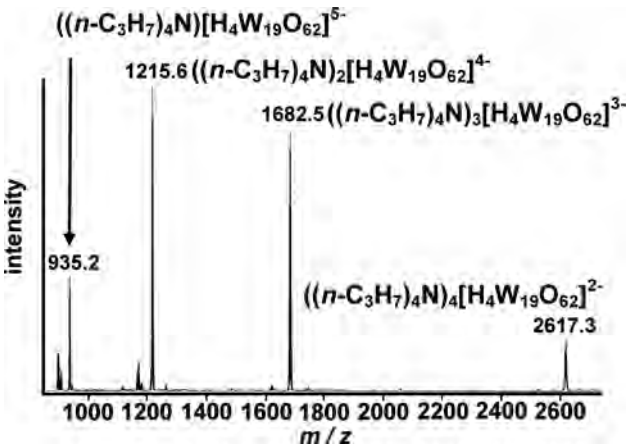

Fig. 6 ESI-MS data of $((n\text{-}C_3H_7)_4N)_6[\alpha\text{-}H_4W_{18}O_{56}(W^{VI}O_6)]\cdot 6CH_3CN$ in acetonitrile showing the plenary cluster fragments observed, from doubly-charged peak $((n\text{-}C_3H_7)_4N)_4[\alpha\text{-}H_4W_{19}O_{62}]^{2-}$ (m/z 2617.3) to $((n\text{-}C_3H_7)_4N)[H_4W_{19}O_{62}]^{5-}$ (m/z 935.2).

negatively charged parent plenary polyanion and compare and contrast these values to see if a general trend can be postulated. The first important observation is that the {γ*-W_{18}Te} tellurite-based Wells–Dawson proved to be the least stable under the experimental conditions (see Table S7†) and fragmented at with a collision energy of 15 eV; whereas the corresponding {γ*-W_{19}} isomer appeared to be the most stable, fragmenting completely at 75 eV. The CID fragmentation experiments, based on the collision energies required to fully fragment the triply charged parent polyanions, showed the following trend in order of decreasing stability: {γ*-W_{19}} > {α-W_{19}} > {β*-W_{18}I} > {γ*-W_{18}Te} (75 eV > 60 eV > 17 eV > 15 eV respectively). It is interesting to note that, unconventionally, the β* isomer of the {W_{18}} cage is stabilised by the presence of the $[IO_6]^{5-}$ contained within and following several years of research into the WD anions, we have been unable to isolate any other β* isomers of this cage.

It is important to add that CID studies cannot be used as the sole means to elucidate mechanistic pathways directly, since the process involves the decomposition of the cluster, but key information can be gathered which will of course be useful to postulate some ideas that can be used to form testable self-assembly hypotheses. It must therefore be noted that, in addition to the parent polyanions, only isopoly fragments were found in the CID mass spectral data, for example commonly $[W_4O_{13}]^{2-}$ up to $[W_{13}O_{40}]^{2-}$ and in the case of {W_{19}} up to $[W_{19}O_{58}]^{2-}$. These observations give us valuable information regarding the potential mechanism of formation of the {W_{18}X} systems as well as the stability of the synthons that exist in solution. It would appear that several isopolyanionic fragments form initially followed by the incorporation of the central {XO_6} template (where X = W, I, Te) which then undergo further aggregation to form the final product through a simple condensation process. This trend is in keeping with the idea that small isonuclear fragments are much more stable, or less labile, in tungsten-based systems, meaning that template anions may be incorporated at a later stage in the aggregation process.[34] A recent publication by us which has analysed the aggregation processes leading towards the assembly of the Keggin anion $[XM_{12}O_{40}]^{q-}$ also concludes that the heteroanion, $[XO_2(OH)_2]^-$, is not incorporated into the polyanion initially.[36a)]

Table 4 compares the Fragmentation Energies (FEs) for γ*-{TeW_{18}}, β*-{IW_{18}}, α- and γ*-{W_{19}} clusters obtained in ESI-MS experiments with Binding Energies (BEs) or atomization energies computed for the non-protonated species. Bridgeman and Cavigliasso have shown that insight into the bonding in POMs can be afforded using atomization energies.[37] We are aware of the fact that to compare FEs and BEs is not straightforward, since the former measures the fragmentation energy to give some specific fragments whereas the latter measures the total decomposition of the anion in atoms. We think, however, that the absolute magnitudes may yield some qualitative information regarding the tendency of the clusters to decompose. For instance both DFT and experimental data show that {W_{19}} clusters are more stable than {TeW_{18}}, which decomposes at a much lower energy. Further analysis must be performed to both explore and validate this postulate so to carefully compare and extract information from both experimental ESI-MS and DFT bonding energy analysis.

Table 4 Theoretical DFT Binding Energy (BE) in eV for the observed isomers and a summary the energy required for the total fragmentation of the cluster in the ESI-MS experiments, Fragmentation Energy (FE)

	DFT (eV)		Experimental (eV)	
Isomers	BE[a]	ΔE_{BE}	FE[b]	ΔE_{FE}
γ*-$[W_{18}O_{56}(TeO_6)]^{10-}$	−458.9	12	15	60
β*-$[W_{18}O_{56}(IO_6)]^{9-}$	−468.6	3	17	58
α-$[W_{18}O_{56}(WO_6)]^{10-}$	−470.5	1	60	5
γ*-$[W_{18}O_{56}(WO_6)]^{10-}$	−471.2	0	75	0

[a] B.E. (Binding Energy) in gas phase. [b] F.E. (Fragmentation Energy) in gas phase

Conclusions

The classical Wells–Dawson anions can be synthesised as different isomers α, β, γ, α*, β* and γ* according to the relative disposition of atoms. DFT confirmed that in classical WD anions the stability order is α > β > γ > γ*≫ α*> β*. The largest instability of α* and β* explains why these two isomers have yet to be observed. ESI-MS and DFT studies have been carried out to analyse the relative stability for a series of non-classical WD anions. In contrast, for the non-classical WD anions the obtained DFT stability order is γ* > β* > α* > α ≫ β > γ where the isomers γ*, β* and α are the only anions of this type known to have been synthesised so far. The collision energy necessary to induce the total fragmentation of the {XW_{18}} parent polyanion by ESI-MS was always found to be lower than the homologous {W_{19}} species; binding energies predicted by DFT are in agreement with this general trend. We have been able to rationalise the isomerism in this new class of WD anions and explain their preference to adopt certain isomer-structures. In future, we aim to perform detailed analyses on the influence of the redox properties on isomer stability.

Computational and mass spectra details

Computational methodology. The calculations were carried out using DFT methodology with the program package ADF (Amsterdam Density Functional).[38] The gradient-corrected functionals of Becke[39] and Perdew[40] for the exchange and correlation energies, respectively, were used to improve the description of the electronic density provided by the local density approximation (X-alpha functional for the exchange part and Vosko–Wilk–Nusair functional for the correlation part).[41] The valence electrons for all atoms were described with Slater-type basis function of triple-ζ plus polarisation quality. The inner electrons have been kept frozen. Scalar relativistic corrections were included by means of the zeroth-order regular approximation (ZORA) formalism. All the computed geometries have closed-shell electronic structure. The present computational settings, BP86/TZP, have been demonstrated to be a satisfactory methodology for describing the electronic structure of polyoxometalates.[42] All the structures discussed through this work were fully optimized taking into account the solvent effects by means of a continuous model. We have used the Conductor-like Screening Model (COSMO)[43] as implemented in ADF[44] program package. To define the cavity that surrounds the molecules we use the solvent accessible surface (SES) method and a fine tesserae. To obtain the electron density in solution, first it is converged in the gas phase and afterward the COSMO model is turned on to include the solvent effects

variationally. The ionic radii of the atoms, which define the dimensions of the cavity surrounding the molecule, are chosen to be 1.26 Å for W, 0.64 for Mo, 1.52 for O, 1.20 for H, 2.10 for Si, 1.00 for P, 0.56 for As, 0.30 for S, 0.78 for I and 0.81 for Te. The dielectric constant (ε) is set to 78 so as to model water as solvent.

Experimental section

General considerations: all commercially obtained reagents were used without any further purification. Deionised water was used throughout the study.

Synthesis: For the ESI-MS fragmentation experiments, $((n\text{-}C_3H_7)_4N)_6[\alpha\text{-}H_4W_{18}O_{56}(W^{VI}O_6)]\cdot 6CH_3CN$, $((n\text{-}C_3H_7)_4N)_6[\gamma^*\text{-}H_4W_{18}O_{56}(W^{VI}O_6)]\cdot 3CH_3CN$, $((n\text{-}C_3H_7)_4N)_6[\beta^*\text{-}H_3W_{18}O_{56}(I^{VII}O_6)]$ and $((n\text{-}C_3H_7)_4N)_7[\gamma^*\text{-}H_3W_{18}O_{56}(Te^{VI}O_6)]\cdot 4CH_3CN$ were synthesised using the reported procedures, see Ref. 11–13. Their identities were confirmed by single-crystal X-ray diffraction and elemental analysis.

CID-MS fragmentation experiments and analyses: all MS data were collected using a Q-trap, time-of-flight MS (MicrOTOF-QMS) instrument equipped with and electrospray ionisation (ESI) source supplied by Bruker Daltonics Ltd. The detector was a time-of-flight, 150 microchannel plate detector, and all data were processed using the Bruker Daltonics Ltd. Data Analysis 4.0 software; while simulated isotope patterns were investigated using Bruker Isotope Pattern software and Molecular Weight Calculator 6.45. The following parameters were consistent for all CID-MS scans given below. The calibration solution used was Agilent ES tuning mix solution (Recorder No. G2421A) enabling calibration between approximately 100 m/z and 3000 m/z. This solution was diluted 50 : 1 with MeCN. Samples were introduced into the MS *via* direct injection at a rate of 180 μL h^{-1}. The Quadrupole settings were the same for all samples with values as follows: the ion polarity for all MS scans recorded was negative, at 180 °C, with the voltage of the capillary tip set at 4000 V, the end plate offset at 500 V, a transfer time of 120 μs and Pre-Pulse Storage Time of 10 μs. Funnel 1 RF was set at 300 Vpp, and funnel 2 RF at 400 Vpp; while the collision cell RF was set to 1000 Vpp. The collision energy was increased gradually from an initial value of 0 eV up to the value required to completely fragment the triply charged peak—the maximum was 75 eV in the case of $\{\gamma^*\text{-}W_{19}\}$. See supporting information for more details on MS parameters and the data collection runs carried out.†

Acknowledgements

This work was supported by the ESPRC, The University of Glasgow, WestCHEM, the Leverhulme Trust. L.C. thanks the Wolfson Foundation/Royal Society for a merit award. We also acknowledge support from the Spanish MICINN (CTQ2008-06549-C02-01/BQU), the Generalitat de Catalunya (2009SGR-00462) and the XRTQC. X. L. wishes to acknowledge the Ramón y Cajal program (RYC-2008-02493)

Notes and references

1 M. T. Pope, *Heteropoly and Isopoly Oxometalates*, Springer-Verlag, New York, 1983.
2 (*a*) A. Müller and S. Roy, *Coord. Chem. Rev.*, 2003, **245**, 153–166; (*b*) A. Müller, P. Kögerler and C. Kuhlmann, *Chem. Commun.*, 1999, 1347–1658.
3 W. B. Kim, T. Voitl, G. J. Rodríguez-Rivera, S. T. Evans and J. A. Dumesic, *Angew. Chem., Int. Ed.*, 2005, **44**, 778–792.
4 (*a*) P. J. S. Richardt, R. W. Gable, A. M. Bond and A. G. Wedd, *Inorg. Chem.*, 2001, **40**, 703–709; (*b*) T. Ruther, V. M. Hultgren, B. P. Timko, A. M. Bond, W. R. Jackson and A. G. Wedd, *J. Am. Chem. Soc.*, 2003, **125**, 10133–10143.
5 D.-L. Long, R. Tsunashima and L. Cronin, *Angew. Chem., Int. Ed.*, 2010, **49**, 1736–1758.
6 (*a*) J. F. Keggin, *Proc. R. Soc. London, Ser. A*, 1934, **144**, 75–100; (*b*) J. F. Keggin, *Nature*, 1933, **131**, 908–909.
7 (*a*) B. Dawson, *Acta Crystallogr., Sect. B.*, 1953, **6**, 113–126; (*b*) R. Strandberg, *Acta Chem. Scand., Ser. A*, 1975, **29a**, 350–358.
8 (*a*) R. Acerte, C. Hammer and L. C. Baker, *Inorg. Chem.*, 1984, **23**, 1478–1484; (*b*) H. Ichida and Y. Sasaki, *Acta Crystallogr., Sect. C: Cryst. Struct. Commun.*, 1983, **39**, 529–533; (*c*) R. Contant and R. Thouvenot, *Inorg. Chim. Acta*, 1993, **212**, 41–50.
9 N. Fay, A. M. Bond, C. Baffert, J. F. Boas, J. R. Pillbrow, D.-L Long and L. Cronin, *Inorg. Chem.*, 2007, **46**, 3502–3510.
10 H. N. Miras, D. Stone, D.-L. Long, E. J. L. McInnes, P. Köegerler and L. Cronin, *Inorg. Chem.*, 2011, **50**, 8384–8391.
11 (*a*) D.-L. Long, P. Kögerler, A. D. C. Parenty, J. Fielden and L. Cronin, *Angew. Chem.*, 2006, **118**, 4916–4921; (*b*) C. Ritchie, E. M. Burkholder, D.-L. Long, D. Adam, P. Kögerler and L. Cronin, *Chem. Commun.*, 2007, 468–470.
12 D.-L. Long, Y. F. Song, E. F. Wilson, P. Kögerler, S. X. Guo, A. M. Bond, J. S. J. Hargreaves and L. Cronin, *Angew. Chem., Int. Ed.*, 2008, **47**, 4384–4387.
13 J. Yan, D.-L. Long, E. F. Wilson and L. Cronin, *Angew. Chem., Int. Ed.*, 2009, **48**, 4376–4380.
14 L. C. W. Baker and J. S. Figgis, *J. Am. Chem. Soc.*, 1970, **92**, 3794–3797.
15 G. Hervé and A. Tézé, *Inorg. Chem.*, 1977, **16**, 2115–2117.
16 A. F. Wells, *Structural Inorganic Chemistry*, Oxford University Press, Oxford, 1st edn, 1945, pp. 344.
17 M. T. Pope, *Comprehensive Coordination Chemistry II: From Biology to Nanotechnology*, ed. A. G. Wedd, Elsevier, Oxford, 2004, vol. 4, pp. 635–678.
18 A. F. Wells, *Structural Inorganic Chemistry*, Oxford University Press, Oxford, 2nd edn, 1962, pp. 445.
19 (*a*) X. López, C. Bo and J. M. Poblet, *J. Am. Chem. Soc.*, 2002, **124**, 12574–12582; (*b*) B. Keita, B. Levy, L. Nadjo and R. Contant, *New J. Chem.*, 2002, **26**, 1314–1319.
20 F.-Q. Zhang, W. Guan, L.-K. Yan, Y.-T. Zhang, M.-T. Xu, E. Hayfron-Benjamin and Z.-M. Su, *Inorg. Chem.*, 2011, **50**, 4967–4977.
21 C. P. Pradeep, D.-L. Long, P. Kögerler and L. Cronin, *Chem. Commun.*, 2007, 4254–4256.
22 D.-L. Long, C. Streb, Y. F. Song, S. Mitchell and L. Cronin, *J. Am. Chem. Soc.*, 2008, **130**, 1830–1832.
23 (*a*) R. I. Maksimovskaya and G. M. Maksimov, *Russ. J. Inorg. Chem.*, 1995, **40**, 1319–1328; (*b*) R. I. Maksimovskaya and G. M. Maksimov, *Russ. J. Inorg. Chem.*, 1995, **40**, 1313–1318.
24 H. Neubert and J. Fuchs, *Z. Naturforsch. B: Chem. Sci.*, 1987, **42**, 951–958.
25 P. J. S. Richardt, R. W. Gable, A. M. Bond and A. G. Wedd, *Inorg. Chem.*, 2001, **40**, 703–709.
26 H. D'Amour, *Acta Crystallogr., Sect. B: Struct. Crystallogr. Cryst. Chem.*, 1976, **32**, 729–740.
27 (*a*) S. Himeno, T. Hori and A. Saito, *Bull. Chem. Soc. Jpn.*, 1989, **62**, 2184–2188; (*b*) T. Hori, O. Tamada and S. Himeno, *J. Chem. Soc., Dalton Trans.*, 1989, 1491–1497; (*c*) D. M. Way, J. B. Cooper, M. Sadek, T. Vu, P. J. Mahon, A. M. Bond, R. T. C. Brownlee and A. G. Wedd, *Inorg. Chem.*, 1997, **36**, 4227–4233; (*d*) J. Zhang and A. M. Bond, *Inorg. Chem.*, 2004, **43**, 8263–8271; (*e*) R. Neier, C. Trojanowski and R. Mattes, *J. Chem. Soc., Dalton Trans.*, 1995, 2521–2528.
28 Y. Ozawa and Y. Sasaki, *Chem. Lett.*, 1987, 923–926.
29 Y. Jeannin and J. Martin-Frere, *Inorg. Chem.*, 1979, **18**, 3010–3014.
30 C. Baffert, S. C. Feldberg, A. M. Bond, D.-L. Long and L. Cronin, *Dalton Trans.*, 2007, 4599–4607.
31 U. Kortz and M. T. Pope, *Inorg. Chem.*, 1994, **33**, 5643–5646.
32 (*a*) H. N. Miras, J. Yan, D.-L. Long and L. Cronin, *Angew. Chem., Int. Ed.*, 2008, **47**, 8420–8423; (*b*) E. F. Wilson, H. Abbas, B. J. Duncombe, C. Streb, D.-L. Long and L. Cronin, *J. Am. Chem. Soc.*, 2008, **130**, 13876–13884; (*c*) C. P. Pradeep, D.-L. Long, G. N. Newton, Y.-F. Song

and L. Cronin, *Angew. Chem., Int. Ed.*, 2008, **47**(23), 4388–4391; (*d*) H. N. Miras, D. J. Stone, E. J. L. McInnes, R. G. Raptis, P. Baran, G. I. Chilas, M. P. Sigalas, T. A. Kabanos and L. Cronin, *Chem. Commun.*, 2008, 4703–4305; (*e*) H. N. Miras, E. F. Wilson and L. Cronin, *Chem. Commun.*, 2009, 1297–1311; (*f*) H. N. Miras, E. F. Wilson, M. H. Rosnes and L. Cronin, *Angew. Chem., Int. Ed.*, 2011, **50**, 3720–3724; (*g*) D.-L. Long, P. Kögerler, J. Farrugia and L. Cronin, *Angew. Chem., Int. Ed.*, 2003, **42**, 4180–4183.

33 (*a*) M. J. Deery, O. W. Howarth and K. R. J. Jennings, *J. Chem. Soc., Dalton Trans.*, 1997, (24), 4783–4788; (*b*) T. Waters, R. A. J. O'Hair and A. G. Wedd, *J. Am. Chem. Soc.*, 2003, **125**, 3384–3396; (*c*) C. A. Ohlin, E. M. Villa, J. C. Fettinger and W. H. Casey, *Angew. Chem., Int. Ed.*, 2008, **47**, 8251–8254.

34 H. N. Miras, D. Stone, D.-L. Long, E. J. L. McInnes, P. Kögerler and L. Cronin, *Inorg. Chem.*, 2011, **50**, 8384–8391.

35 M. T. Ma, T. Waters, K. Beyer, R. Palamarczuk, P. J. Richardt, R. A. J. O'Hair and A. G. Wedd, *Inorg. Chem.*, 2009, **48**, 598–606.

36 (*a*) L. Vilà-Nadal, S. G. Mitchell, A. Rodríguez-Fortea, H. N. Miras, L. Cronin and J. M. Poblet, *Phys. Chem. Chem. Phys.*, 2011, **13**, 20136–20145; (*b*) L. Vilà-Nadal, A. Rodríguez-Fortea, L.-K. Yan, E. F. Wilson, L. Cronin and J. M. Poblet, *Angew. Chem., Int. Ed.*, 2009, **48**, 5452–5456; (*c*) L. Vilà-Nadal, E. F. Wilson, H. N. Miras, A. Rodríguez-Fortea, L. Cronin and J. M. Poblet, *Inorg. Chem.*, 2011, **50**, 7811–7819.

37 (*a*) A. J. Bridgeman and G. Cavigliasso, *J. Phys. Chem. A*, 2003, **107**, 4568–4577; (*b*) A. J. Bridgeman and G. Cavigliasso, *Faraday Discuss.*, 2003, **124**, 239–258.

38 (*a*) ADF 2008. 01, SCM, Theoretical Chemistry, Vrije Universiteit, Amsterdam, The Netherlands (http://www.scm.com); (*b*) G. te Velde, F. M. Bickelhaupt, S. J. A. van Gisbergen, C. Fonseca Guerra, E. J. Baerends, J. G. Snijders and T. Ziegler, *J. Comput. Chem.*, 2001, **22**, 931–967.

39 (*a*) A. D. Becke, *J. Chem. Phys.*, 1986, **84**, 4524–4529; (*b*) A. D. Becke, *Phys. Rev.*, 1988, **A38**, 3098–3100.

40 (*a*) J. P. Perdew, *Phys. Rev*, 1986, **B33**, 8822–8824; (*b*) J. P. Perdew, *Phys. Rev.*, 1986, **B34**, 7406–7406.

41 S. H. Vosko, L. Wilk and M. Nusair, *Can. J. Phys.*, 1980, **58**, 1200–1211.

42 (*a*) J. M. Poblet, X. López and C. Bo, *Chem. Soc. Rev.*, 2003, **32**, 297–308; (*b*) X. López, J. M. Maestre, C. Bo and J. M. Poblet, *J. Am. Chem. Soc.*, 2001, **123**, 9571–9576; (*c*) X. López, J. A. Fernández, S. Romo, J. F. Paul, L. Kazansky and J. M. Poblet, *J. Comput. Chem.*, 2004, **25**, 1542–1549; (*d*) X. López, P. Miró, J. J. Carbó, A. Rodríguez-Fortea, C. Bo and J. M. Poblet, *Theor. Chem. Acc.*, 2011, **128**, 393–404.

43 (*a*) A. Klamt and G. J. Schüürmann, *J. Chem. Soc., Perkin Trans. 2*, 1993, (5), 799–800; (*b*) J. Andzelm, C. Kölmel and A. Klamt, *J. Chem. Phys.*, 1995, **103**, 9312–9320; (*c*) A. Klamt, *J. Phys. Chem.*, 1995, **99**, 2224–2235.

44 C. C. Pye and T. Ziegler, *Theor. Chem. Acc.*, 1999, **101**, 396–408.